Molecular Neurobiology
https://doi.org/10.1007/s12035-022-02904-5

P. edulis Extract Protects Against Amyloid-β Toxicity in Alzheimer's Disease Models Through Maintenance of Mitochondrial Homeostasis via the FOXO3/DAF-16 Pathway

Shu-qin Cao[1,2] · Yahyah Aman[2] · Evandro F. Fang[2,3] · Tewin Tencomnao[4,5]

Received: 28 December 2021 / Accepted: 26 May 2022
© The Author(s), under exclusive licence to Springer Science+Business Media, LLC, part of Springer Nature 2022

Abstract

Alzheimer's disease (AD) is a common and devastating disease characterized by pathological aggregations of beta-amyloid (Aβ) plaques extracellularly, and Tau tangles intracellularly. While our understandings of the aetiologies of AD have greatly expanded over the decades, there is no drug available to stop disease progression. Here, we demonstrate the potential of *Passiflora edulis* (*P. edulis*) pericarp extract in protecting against Aβ-mediated neurotoxicity in mammalian cells and *Caenorhabditis elegans* (*C. elegans*) models of AD. We show *P. edulis* pericarp protects against memory deficit and neuronal loss, and promotes longevity in the Aβ model of AD via stimulation of mitophagy, a selective cellular clearance of damaged and dysfunctional mitochondria. *P. edulis* pericarp also restores memory and increases neuronal resilience in a *C. elegans* Tau model of AD. While defective mitophagy-induced accumulation of damaged mitochondria contributes to AD progression, *P. edulis* pericarp improves mitochondrial quality and homeostasis through BNIP3/DCT1-dependent mitophagy and SOD-3-dependent mitochondrial resilience, both via increased nuclear translocation of the upstream transcriptional regulator FOXO3/DAF-16. Further studies to identify active molecules in *P. edulis* pericarp that could maintain neuronal mitochondrial homeostasis may enable the development of potential drug candidates for AD.

Keywords Alzheimer's disease · Glutamatergic neurons · DAF-16 · Mitophagy · DCT-1

Introduction

Alzheimer's disease (AD) is a progressive and irreversible disease of the central nervous system (CNS). It is the most common form of dementia affecting around 50 million people globally at present, a figure estimated to triple by 2050 [1]. Clinically, it is characterized by an insidious onset and progressive deterioration of cognitive function [1, 2]. The pathological hallmarks of the disease include formation of extracellular plaques composed of aggregated beta-amyloid (Aβ) and accumulation of intracellular Tau in the form of neurofibrillary tangles [3–7]. These pathological features are accompanied by neuroinflammation, mitochondrial dysfunction, synaptic degeneration, and neuronal loss due to necroptosis [8–13]. To date, cholinesterase inhibitors and glutamate receptor antagonists have been the standard drugs for the treatment of AD. These therapeutic interventions provide symptomatic relief, but are incapable of curing and/or delaying the progression of the disease. Therefore, there is a dire need for identification of novel therapeutic strategies to counter AD.

✉ Evandro F. Fang
e.f.fang@medisin.uio.no

✉ Tewin Tencomnao
tewin.t@chula.ac.th

1 Ph.D. Program in Clinical Biochemistry and Molecular Medicine, Department of Clinical Chemistry, Faculty of Allied Health Sciences, Chulalongkorn University, Bangkok 10330, Thailand

2 Department of Clinical Molecular Biology, University of Oslo and Akershus University Hospital, 1478 Lørenskog, Norway

3 The Norwegian Centre On Healthy Ageing (NO-Age), Oslo, Norway

4 Department of Clinical Chemistry, Faculty of Allied Health Sciences, Chulalongkorn University, Bangkok 10330, Thailand

5 Natural Products for Neuroprotection and Anti-Ageing Research Unit, Chulalongkorn University, Bangkok 10330, Thailand

Revised Proof

Passiflora edulis (*P. edulis*), commonly known as passion fruit, is native to Southern America, but widely cultivated in tropical and subtropical areas worldwide. The pulp and pericarp of the passion fruit are a source of phytochemical contents such as polyphenols, triterpenoids, glycosides, carotenoids, polysaccharides, aromatic oils, and essential nutrients [14–18]. Pharmacological studies have identified the bioactivities of passion fruit including anti-oxidative, anti-inflammatory, anti-diabetic, and potentially hepatoprotective effects [19–23]. Additionally, it has been reported that passion fruit extracts act as a modulator of the glutamatergic system, which further promotes neuroprotective activities [24, 25]. However, the underlying mechanism of the neurotherapeutic activity of *P. edulis* extract has remained elusive. In this study, we wanted to determine whether administration of *P. edulis* extract could inhibit memory loss and pathological phenotypes in *Caenorhabditis elegans* (*C. elegans*) models of AD. We further evaluated the underlying molecular mechanisms in both *C. elegans* and mammalian cell systems.

Results

P. edulis Pericarp Extract Attenuates Memory Loss and Prolongs Lifespan in AD *C. elegans*

Progressive memory impairment is the most common symptom in AD patients [26]. Thus, we set out to evaluate whether the *P. edulis* pericarp (PEP) extract can inhibit memory loss in the transgenic *C. elegans* models of AD harboring pan-neuronal human $A\beta_{1\text{-}42}$ (JKM2, $hA\beta_{1\text{-}42}$) or pan-neuronal expression of human P301L Tau mutation (CK12, hTau[P301L]). For this purpose, we utilized an aversive olfactory learning chemotaxis assay (a negative value correlates with positive chemotaxis-related memory). Transgenic nematodes expressing $hA\beta_{1\text{-}42}$ and hTau[P301L] displayed severe cognitive deficits and neurodegeneration as we [10, 27] and others [28, 29] reported before. We administrated PEP at 250 µg/ml to the nematodes from egg hatching onwards and performed memory experiments on adult day 1. While the $hA\beta_{1\text{-}42}$ and hTau[P301L] animals had impaired memory, PEP inhibited memory loss in these AD nematodes; to note, PEP did not influence the memory of WT (N2) animals (Fig. 1a). Epidemiological studies indicate that AD not only impairs memory but also shortens lifespan [30, 31]. We postulated that strategies that improve memory in animals with AD could also extend their lifespan [27]. Therefore, we subsequently assess the potential effect of PEP on lifespan in the transgenic nematode models of AD. As expected, in the transgenic *C. elegans* models of AD, especially, the hTau[P301L] model exhibited a shorter lifespan in comparison to WT control (Fig. 1b). Upon PEP administration, not only hTau[P301L] and $hA\beta_{1\text{-}42}$ nematodes displayed a significant extension of lifespan, but also elongate the lifespan of the WT animals (Fig. 1c–e). Along with lifespan, we also evaluated pharyngeal pumping in adult day 2 and day 8 animals. PEP supplementary with no influence on pumping rate (Fig. 1f, h) indicated that PEP extended lifespan not due to the starvation. A summary of the lifespan data in different groups is shown in Supplementary Table 1. These findings indicate PEP protected against memory deficits and extended lifespan in particular the $hA\beta_{1\text{-}42}$ model of AD.

P. edulis Extract Inhibits Neurodegeneration in AD *C. elegans* and Cells

Having established the potential of PEP extract to improve healthspan and lifespan in the *C. elegans* $hA\beta_{1\text{-}42}$ model of AD, we set out to investigate the underlying mechanism. For this purpose, we first evaluated whether PEP potentiates neuroprotection that results in the improved functional behavior. The two major neurotransmission systems primarily affected in AD are the cholinergic and the glutamatergic systems [32–34]. Cholinergic neurons play a key role in the CNS, and acetylcholine (ACh) works as a neurotransmitter that serviced all cholinergic neurons. There is a likelihood that either Ach depletion or hyper-accumulation links to neurodegeneration [35–37]. The functional activity of the cholinergic system in the AD nematodes was assessed by feeding the animals with aldicarb, an acetylcholinesterase inhibitor that induces hyper-accumulation of Ach, resulting in accelerated skeletal muscle contraction and finally paralysis [38]. Controls for the assay, in the form of aldicarb hypersensitive (VC233: *tom-1(ok285)I*) and aldicarb-resistant (NM204: *snt-1(md290)II*) strains, displayed increased and reduced sensitivities to aldicarb, respectively, compared to the WT nematodes (Fig. 2a). The $hA\beta_{1\text{-}42}$ model of AD displayed an increased sensitivity to aldicarb compared to the WT N2; while hTau[P301L] nematodes did not show increased sensitivity to aldicarb compared to that of WT animals (Fig. 2a). These findings suggest an impairment in the cholinergic system in $hA\beta_{1\text{-}42}$ nematodes. Application of PEP resulted in a delay in aldicarb-mediated paralysis in both $hA\beta_{1\text{-}42}$ and hTau[P301L] models of AD, as well as in the WT N2 nematodes (Fig. 2b–d). This implies that PEP enhanced cholinergic neuronal resistance to aldicarb in both pathological and physiological conditions.

In addition to cholinergic neuronal protection, we asked whether PEP could protect against degeneration of the glutamatergic neurons in AD. Glutamatergic neurons are another vital type of neurons found in the CNS, and are impaired in AD [39, 40]. Aβ induces glutamatergic neuronal loss and promotes AD progresses [40, 41]. To evaluate whether PEP could protect against Aβ-induced neurodegeneration in the glutamatergic subtype neurons, we used a series of

Revised Proof

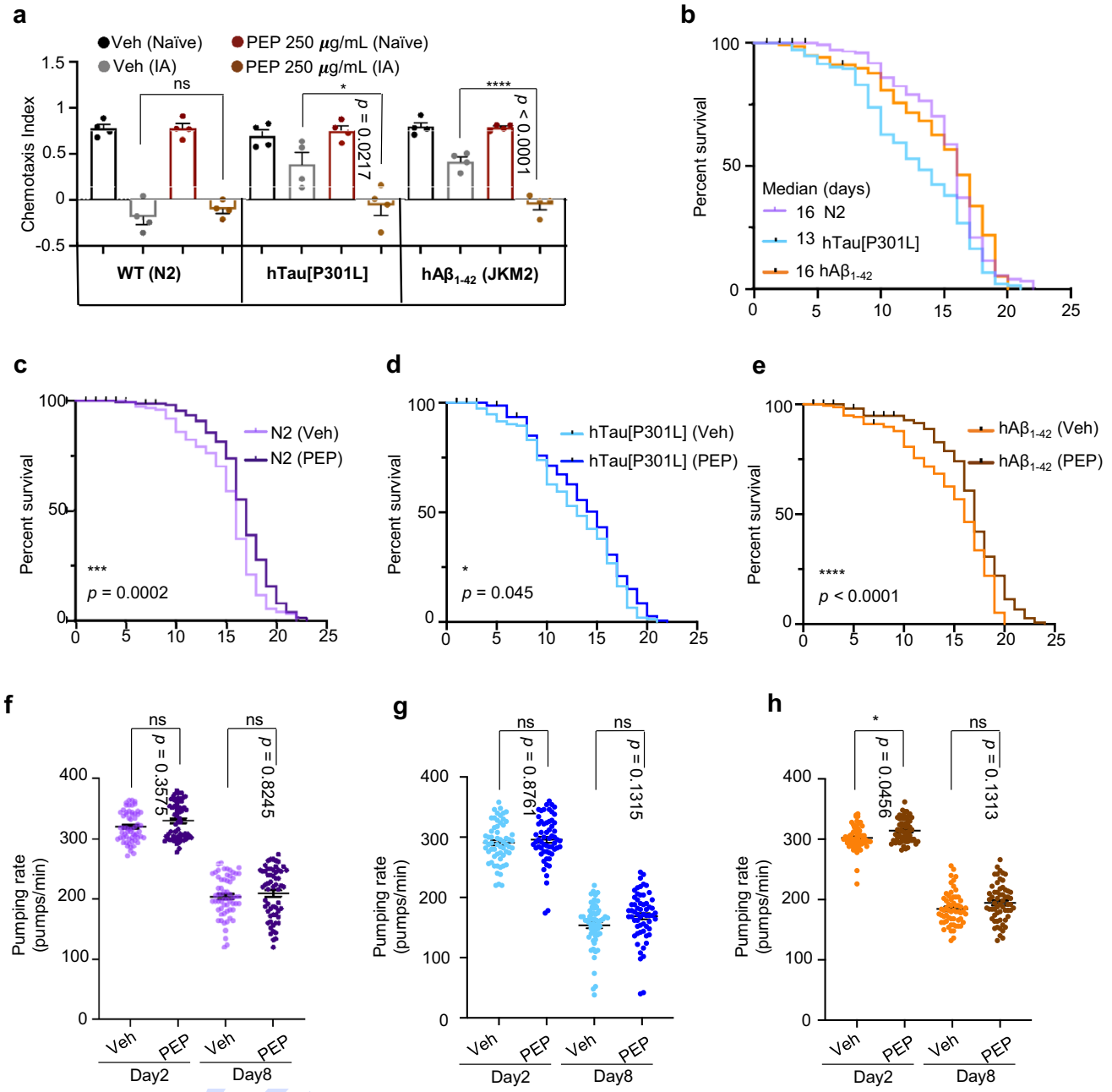

Fig. 1 PEP improves memory and extends lifespan in AD models of *C. elegans*. **a** PEP restored memory in adult day 1 hTau[P301L] and hA$\beta_{1\text{-}42}$ (JKM2) *C. elegans*. Data were from four biological repeats with the results shown in mean ± SEM. One-way ANOVA followed by Tukey's multiple comparisons test was used for data analysis with ns, no significance; *$p < 0.05$, **$p < 0.01$, ***$p < 0.001$, ****$p < 0.0001$. **b** Pathological Tau and A$\beta_{1\text{-}42}$ caused shorter lifespan in hTau[P301L] and hA$\beta_{1\text{-}42}$ (JKM2) nematodes when compare to WT animals. **c–e** PEP extended lifespan in WT (N2), hTau[P301L], and hA$\beta_{1\text{-}42}$ (JKM2) *C. elegans*. Data were pooled from two biological replicates with a total of 150 animals (each biological repeat includes three technical repeats). The Kaplan–Meier survival curves were presented with the log-rank (Mantel-Cox) test used for data analysis. ns, no significance; *$p < 0.05$, **$p < 0.01$, ***$p < 0.001$, ****$p < 0.0001$. **f–h** Effect of PEP on pharyngeal pumping speed in adult day 2 and day 8 WT (N2), hTau[P301L], and hA$\beta_{1\text{-}42}$ (JKM2) *C. elegans*. Data were from two biological replicates with a total 60 animals (each biological repeat includes three technical repeats). One-way ANOVA followed by Tukey's multiple comparisons test was used for data analysis. ns, no significance; *$p < 0.05$

well-characterized nematode models whereby hA$\beta_{1\text{-}42}$ is only expressed in the glutamatergic neurons and induces neurodegeneration [27, 42]. Five tail-localized glutamatergic neurons (LUA(R), LUA(L), PVR, PLM(R), and PLM(L)) were used for data quantification as these five neurons show clear, stable, and easy-to-quantify patterns of neurodegeneration

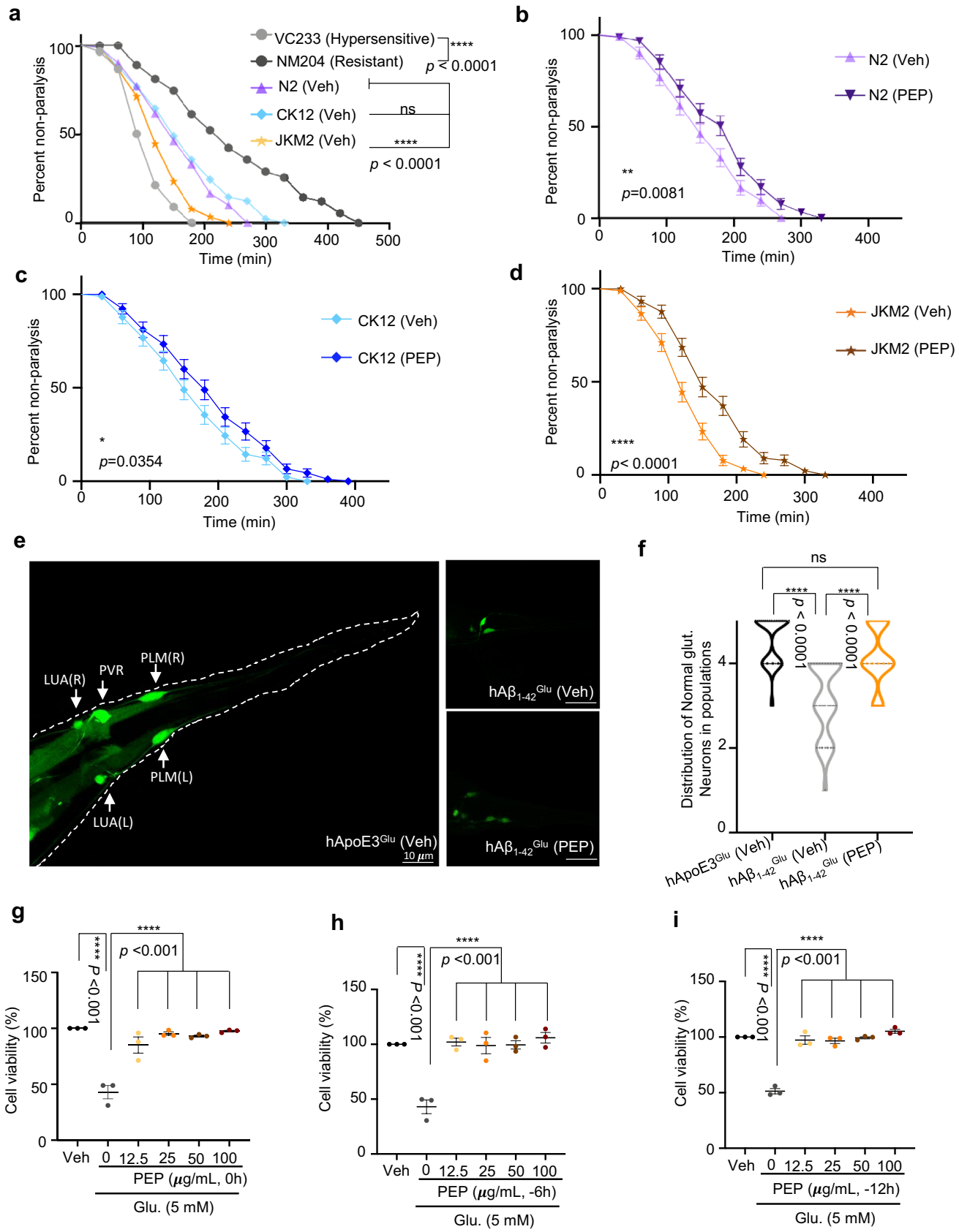
a
VC233 (Hypersensitive)
NM204 (Resistant)
N2 (Veh)
CK12 (Veh)
JKM2 (Veh)
****
p < 0.0001
ns
****
p < 0.0001
Percent non-paralysis
Time (min)
b
N2 (Veh)
N2 (PEP)
**
p=0.0081
Percent non-paralysis
Time (min)
c
CK12 (Veh)
CK12 (PEP)
*
p=0.0354
Percent non-paralysis
Time (min)
d
JKM2 (Veh)
JKM2 (PEP)
****
p< 0.0001
Percent non-paralysis
Time (min)
e
LUA(R)
PVR
PLM(R)
PLM(L)
LUA(L)
hApoE3Glu (Veh)
10 μm
hAβ1-42Glu (Veh)
hAβ1-42Glu (PEP)
f
ns
****
p < 0.0001
****
p < 0.0001
Distribution of Normal glut. Neurons in populations
hApoE3Glu (Veh)
hAβ1-42Glu (Veh)
hAβ1-42Glu (PEP)
g
****
p <0.001
****
P <0.001
Cell viability (%)
Veh
0
12.5
25
50
100
PEP (μg/mL, 0h)
Glu. (5 mM)
h
****
p <0.001
****
P <0.001
Cell viability (%)
Veh
0
12.5
25
50
100
PEP (μg/mL, -6h)
Glu. (5 mM)
i
****
p <0.001
****
P <0.001
Cell viability (%)
Veh
0
12.5
25
50
100
PEP (μg/mL, -12h)
Glu. (5 mM)

◂**Fig. 2** PEP protects cholinergic and glutamatergic neurons in the AD nematodes. **a** Nematodes reacted to the acetylcholinesterase inhibitor (aldicarb). VC233 was an aldicarb hypersensitive strain, while NM204 was an aldicarb-resistant strain. WT (N2), hTau[P301L], and $hA\beta_{1\text{-}42}$ (JKM2) nematodes were test groups. **b–d** PEP increased neuronal resilience (as evidenced by prolonged paralysis time) against aldicarb-induced toxicity in day 1 WT (N2), hTau[P301L], and $hA\beta_{1\text{-}42}$ (JKM2) nematodes. Data were from three biological repeats. Log-rank (Mantel-Cox) test was used for data analysis with ns, no significance; $^{*}p<0.05$, $^{**}p<0.01$, $^{***}p<0.001$, $^{****}p<0.0001$. **e** Representative images showing the condition of glutamatergic neurons in day 3 $hApoE3^{Glu}$ (left), $hA\beta_{1\text{-}42}{}^{Glu}$ (up-right), and $hA\beta_{1\text{-}42}{}^{Glu}$ nematodes under different conditions. **f** PEP protected against Aβ-induced glutamatergic neuronal degeneration in day 3 $hA\beta_{1\text{-}42}{}^{Glu}$ nematodes. Five glutamatergic neurons including LUA(R), LUA(L), PLM(R), PLM(L), and PVR were used for data analysis. Data were from three biological repeats. One-way ANOVA followed by Tukey's multiple comparisons test was used for data analysis with ns, no significance; $^{*}p<0.05$, $^{**}p<0.01$, $^{***}p<0.001$, $^{****}p<0.0001$. **g–i** PEP attenuated high glutamate (5 mM)-induced cell death in HT-22 cells under different conditions. Varied concentrations (12.5–100 μg/ml) of PEP were used in the experiments. Data were from three biological repeats. One-way ANOVA followed by Tukey's multiple comparisons test was used for data analysis with ns, no significance; $^{*}p<0.05$, $^{**}p<0.01$, $^{***}p<0.001$, $^{****}p<0.0001$.

[42]. As reported before [27, 42], transgenic nematodes carrying $hA\beta_{1\text{-}42}$ overexpression in their glutamatergic neurons exhibited significant reduction in glutamatergic neurons in comparison to controls, implicating Aβ-mediated neurodegeneration of glutamatergic neurons in the models of AD (Fig. 2e, f). PEP administration almost completely annulled Aβ-induced neurodegeneration (Fig. 2e, f).

Encouraged by the strong in vivo glutamatergic neuronal protection by PEP, we asked whether this benefit is preserved in mammalian cells including in the HT-22 and SH-SY5Y cells. To this end, mammalian HT-22 mouse hippocampal cells, which are devoid of cholinergic and glutamate receptors, were utilized to evaluate glutamate-induced cell death and examine the neuroprotective effect of PEP via checking cell viability using the MTT assay. Glutamate at 5 mM showed a significant toxicity (around 45%) in the HT-22 cells compared to vehicle control (Fig. 2g–i). Exposing the HT-22 cells to PEP extract as co-treatment with glutamate resulted in a dose-dependent inhibition of HT-22 cell death (Fig. 2g). Furthermore, 6-h and 12-h pretreatment with PEP showed even better cell protection against glutamate toxicity (5 mM, 24 h) (Fig. 2h, i). In addition to using HT-22 cells, we further study neuroprotective effects of PEP using the human fibroblastoma SH-SY5Y cells. We used the two-step retinoic acid (RA) and brain-derived neurotrophic factor (BDNF) protocol and successfully differentiate the SH-SY5Y cells to neuronal-like cells (Supp. Figure 1b–d), followed by Aβ toxicity assay. $A\beta_{25\text{-}35}$ peptides reduced cell viability in dose-dependent manners compared to vehicle control (Supp. Figure 1e). Co-administration of PEP at 100 μg/ml (but not lower doses as we tested), with $A\beta_{25\text{-}35}$ (18 h) or as pretreatment at 6 h (but not 12 h) prior to $A\beta_{25\text{-}35}$ administration (18 h), was sufficient to protect against $A\beta_{25\text{-}35}$-induced neuronal death (Fig. 3a–c), and alleviate $A\beta_{25\text{-}35}$-induced generation of mitochondrial superoxide (Fig. 3d, e). Additionally, PEP pretreatment (6 h ahead) protected against $A\beta_{25\text{-}35}$-induced loss of mitochondrial membrane potential (Fig. 3f, g). Our data suggest PEP not only protects against glutamate-induced cell death, but also protects against $A\beta_{25\text{-}35}$-induced neurotoxicity and neuronal loss in both nematodes and human neuronal-like cells.

P. edulis Extract Increased Neuronal Mitophagy in Human Neurons and *C. elegans*

Compromised mitophagy-induced accumulation of damaged mitochondria in the brain, especially in the entorhinal cortex and the hippocampus, is an early sign and a risk factor of AD [8, 10, 27]. Our previous studies show that genetic or pharmacological restoring of neuronal mitophagy abrogated memory loss and pathologies in AD [10, 27]. Here, we asked whether PEP could induce mitophagy, and if yes, whether PEP-induced memory retention is dependent on mitophagy activation. Mitophagy is a subtype of selective autophagy; thus, there are many proteins participating in both cellular events [43, 44]. For mechanistic exploration, we checked expression levels of proteins critical for the mitophagy and autophagy pathways using the SH-SY5Y-differentiated neuronal-like cells. Immunoblot data showed that PEP (100 μg/ml, 6-h pretreatment) inhibited phosphorylation of the mammalian target of rapamycin (mTOR) (Fig. 4a, b), reduced phosphorylation of ULK1 at p-S757 (activation of this site inhibits ULK1 activity), and increased the expression of mitophagy-related multifunctional protein BNIP3 and the lysosome protein cathepsin D; compared with the $A\beta_{25\text{-}35}$ group, $A\beta_{25\text{-}35}$ + PEP did not have significant effects on the protein levels of PINK1, Parkin, p62, SOD-1, or SOD-2 (Fig. 4a, b).

While the immunoblot data strongly suggest a possibility that PEP affects mitophagy/autophagy proteins, we further designed experiments to validate this possibility. To investigate that PEP could induce mitophagy in neurons, we utilized two composite systems for monitoring mitophagy in vivo [45, 46]. First, we utilized transgenic animals expressing a mitochondria-targeted GFP together with the autophagosomal marker LC3/LGG-1 fused with DsRed [10, 46]. Normally, mitophagy-inducing stimuli encourage the formation of autophagosomes that extensively co-localize with mitochondria [46]. Here, we demonstrate a pronounced induction of mitophagy via formation of autophagosomes consisting of mitochondria upon PEP exposure (Fig. 4c, d). This implies that PEP was able to promote the formation of mito-autophagosomes for mitochondria cargo for degradation via mitophagy. Next, we wanted to establish whether the mitochondria in the autophagosome were indeed degraded. For this purpose, we

Revised Proof

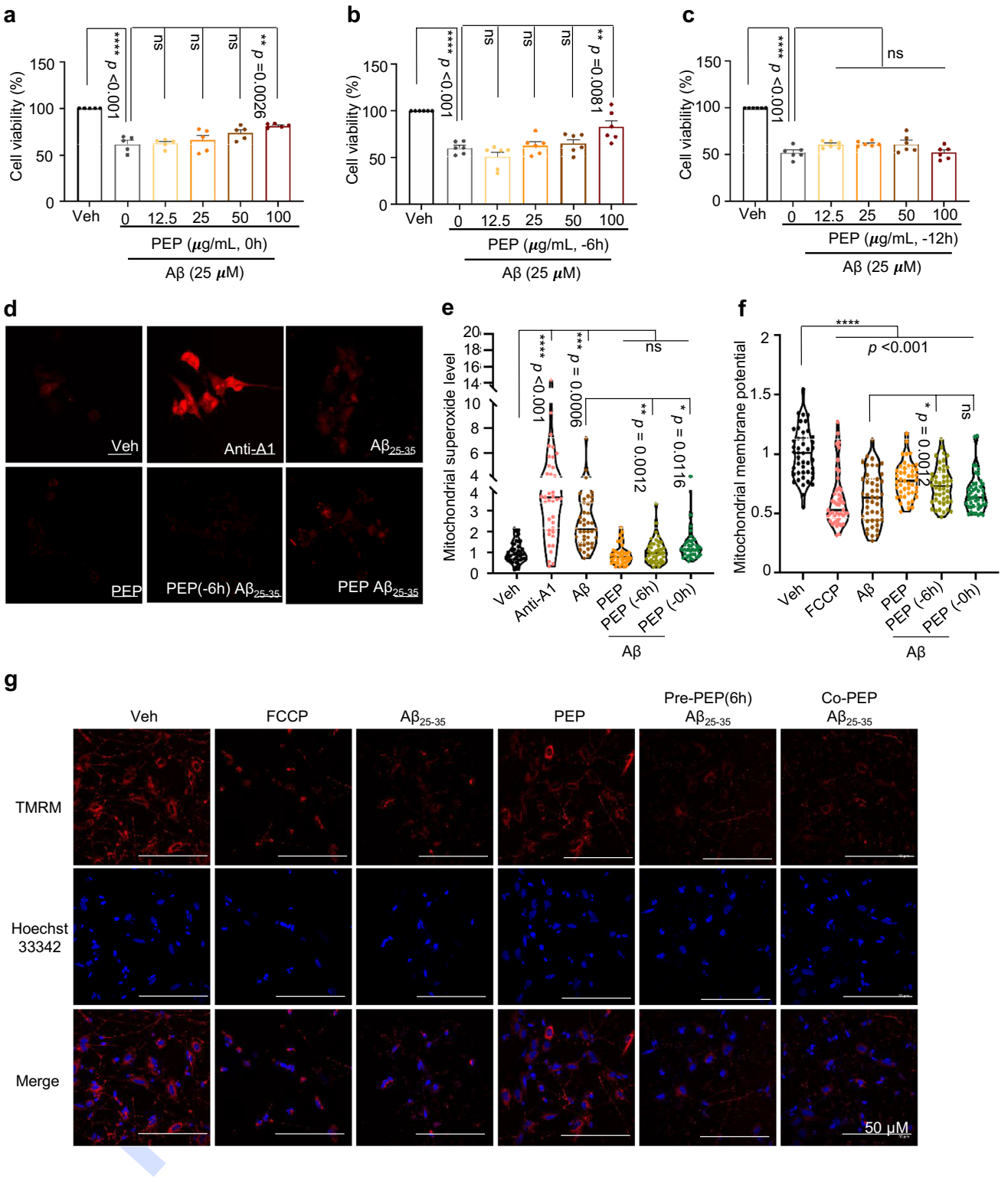

utilized transgenic animals expressing mitochondria-targeted Rosella (mtRosella) biosensor that combines a fast-maturing pH-insensitive DsRed fused to a pH-sensitive green fluorescent protein (GFP) variant [47]. Mechanistically, quenching of the GFP signal upon uptake of the mitochondrial cargo by the acidic lysosome is indicated by a lower GFP/DsRed ratio representing mitophagy stimulation [46]. PEP was indeed able to stimulate mitophagy as the mtRosella animals displayed significantly decreased GFP/DsRed ratio compared to vehicle controls (Fig. 4e, f). Combining the human cell data and the nematode data, we propose PEP stimulates mitophagy via activating the key mitophagy/autophagy protein ULK1, and

◂**Fig. 3** PEP protects against $A\beta_{25-35}$-induced neurotoxicity in human SH-SY5Y-differentiated neuronal-like cells. **a–c** PEP attenuated cell death in SH-SY5Y-differentiated neuronal-like cells under designated conditions. Varied concentrations (12.5–100 μg/mL) of PEP were used in the experiments. Data were from at least three biological repeats. One-way ANOVA followed by Tukey's multiple comparisons test was used for data analysis with ns, no significance; $*p<0.05$, $**p<0.01$, $***p<0.001$, $****p<0.0001$. **d** Representative images showed the oxidized MitoSOX fluorescence signal in control, Antimycin A1 (Anti-A1), $A\beta_{25-35}$, and PEP pre- or co-treated with $A\beta_{25-35}$ in differentiated SHSY5Y cells. Scale bar, 20 μm. **e** PEP alleviated $A\beta_{25-35}$-induced mitochondrial superoxide level. Anti-A1 (100 μM) was used as a positive control. Data were from three biological repeats. One-way ANOVA followed by Tukey's multiple comparisons test was used for data analysis with ns, no significance; $*p<0.05$, $**p<0.01$, $***p<0.001$, $****p<0.0001$. **f** PEP pretreatment (6 h ahead) attenuated $A\beta_{25-35}$-reduced mitochondrial membrane potential. FCCP (20 Mm, 1 h) was used as positive control. Data were from three biological repeats. One-way ANOVA followed by Dunnett's multiple comparisons test was used for data analysis with ns, no significance; $*p<0.05$, $**p<0.01$, $***p<0.001$, $****p<0.0001$. **g** Representative images with TMRM and Hoechst33342 signals. The figures show mitochondrial networks in control, FCCP, $A\beta_{25-35}$, PEP, and PEP pre- or co-treated with $A\beta_{25-35}$ in differentiated SH-SY5Y cells. Red color indicates mitochondrial network; blue color indicates cell nuclei. Scale bar, 50 μm

increasing the expression of both mitophagy-related protein BNIP3 and lysosome protein cathepsin D.

P. edulis Extract Promotes Mitochondrial Homeostasis and Oxidative Resistance via DAF-16 Nuclear Translocation in *C. elegans*

In addition to the mechanism mentioned above, we wondered whether PEP-based neuronal benefits could be started at the transcriptional level. We used real-time PCR and checked the mRNA levels of a list of genes in the groups of "mitophagy," "mitochondrial unfolded protein response (UPR^{mt})," and "oxidative stress," which are linked to neuroprotection [48, 49]. PEP did not induce significant change, despite an upward trend in genes associated with mitophagy (i.e., *pdr-1*, *dct-1*, *lgg-1*, and *skn-1*) in the $hA\beta_{1-42}$ model of AD and in the WT N2 (Fig. 5a, b). However, significant upregulation of genes associated with oxidative stress (*gst-4* and *sod-3*) as well as the mitochondrial unfolded protein response (UPR^{mt}) (*ubl-5*) was observed in the N2 animals (Fig. 5a). While the $hA\beta_{1-42}$ model of AD exhibited upregulation of only *sod-3* upon PEP application (Fig. 5b), SOD-3 has a role in suppressing oxidative stress that underlies mitochondrial and cellular dysfunction [50]. Previous studies reported that DAF-16 (orthologue for the mammalian *FOXO* transcription factors) is the upstream regulator of *gst-4* and *sod-3* [51, 52]. In our nematode system, the expression level of the *daf-16* gene was not changed in either the N2 controls or the $hA\beta_{1-42}$ model of AD (Fig. 5a, b). Therefore, we went on to investigate whether PEP supplementation could promote the nuclear translocation of DAF-16 by using a transgenic nematode with a DAF-16::GFP-tag. A 4-point grading system was utilized for characterizing DAF-16 localization from the cytosol (1) to predominant nuclear localization (4) (Fig. 5c, d). Under physiological conditions, DAF-16 was distributed predominantly in the cytoplasm; however, upon stimulation with heat-shock (a positive control), DAF-16 was mainly localized in the nucleus (Fig. 5c). PEP induced significant nuclear translocation of DAF-16 (Fig. 5c, d). Altogether, our data suggest that PEP upregulates *gst-4* and *sod-3* genes via enhancing subcellular distribution of DAF-16 from the cytoplasm to the nucleus, resulting in increased DAF-16-regulated transcription activity.

P. edulis Extract Induces Neuronal Mitophagy and Protects Against Aβ-Induced Memory Loss Which is daf-16 Dependent

To further investigate whether PEP induces mitophagy in a *daf-16/dct-1/sod-3*-dependent manner or not, we knocked down *daf-16*, *dct-1*, and *sod-3*, respectively, via RNAi feeding of the animals from the egg hatching stage. The $mtRosella^{neu-sid1}$ (to knockdown target only in the neurons but not other tissues) transgenic animals were used in these experiments. Our results show that knock down of *daf-16* abolished PEP-induced neuronal mitophagy in $mtRosella^{neu-sid1}$ animals; similar results were shown in *dct-1* or *sod-3* knocked down animals (Fig. 5e, f). In addition, to investigate whether the neuroprotective effect of PEP is *daf-16* dependent or not, we knocked down the *daf-16* or *sod-3* gene by using RNAi feeding of the animals from egg hatching. $N2^{neu-sid1}$ and $hA\beta_{1-42}$ $(JKM2)^{neu-sid1}$ transgenic animals were used in these experiments, and our results suggested that knock down of *daf-16* gene expression not only caused memory deficits in healthy control $N2^{neu-sid1}$ animals, but also abolished memory restoration ability of PEP extract in both $N2^{neu-sid1}$ and $hA\beta_{1-42}(JKM2)^{neu-sid1}$ animals. However, *sod-3* RNAi only abolished memory restoration of PEP in $hA\beta_{1-42}$ $(JKM2)^{neu-sid1}$ animals but had no effect in healthy control $N2^{neu-sid1}$ animals (Fig. 5g, h). Cumulatively, PEP protects neurons in AD animals via upregulation of the DAF-16/DCT-1/SOD3-dependent mitophagy pathway.

Identification of Potential Bioactive Compounds in *P. edulis* Pericarp

The neuroprotective effect of PEP could be contributed by the small bioactive compounds inside the extracts. To identify small molecules in PEP, we used gas chromatography-mass spectrometry (GC–MS). Over hundreds of compounds have been identified in PEP extract and the list of compounds is shown in Supplementary Table 2. To further narrow down the

Revised Proof

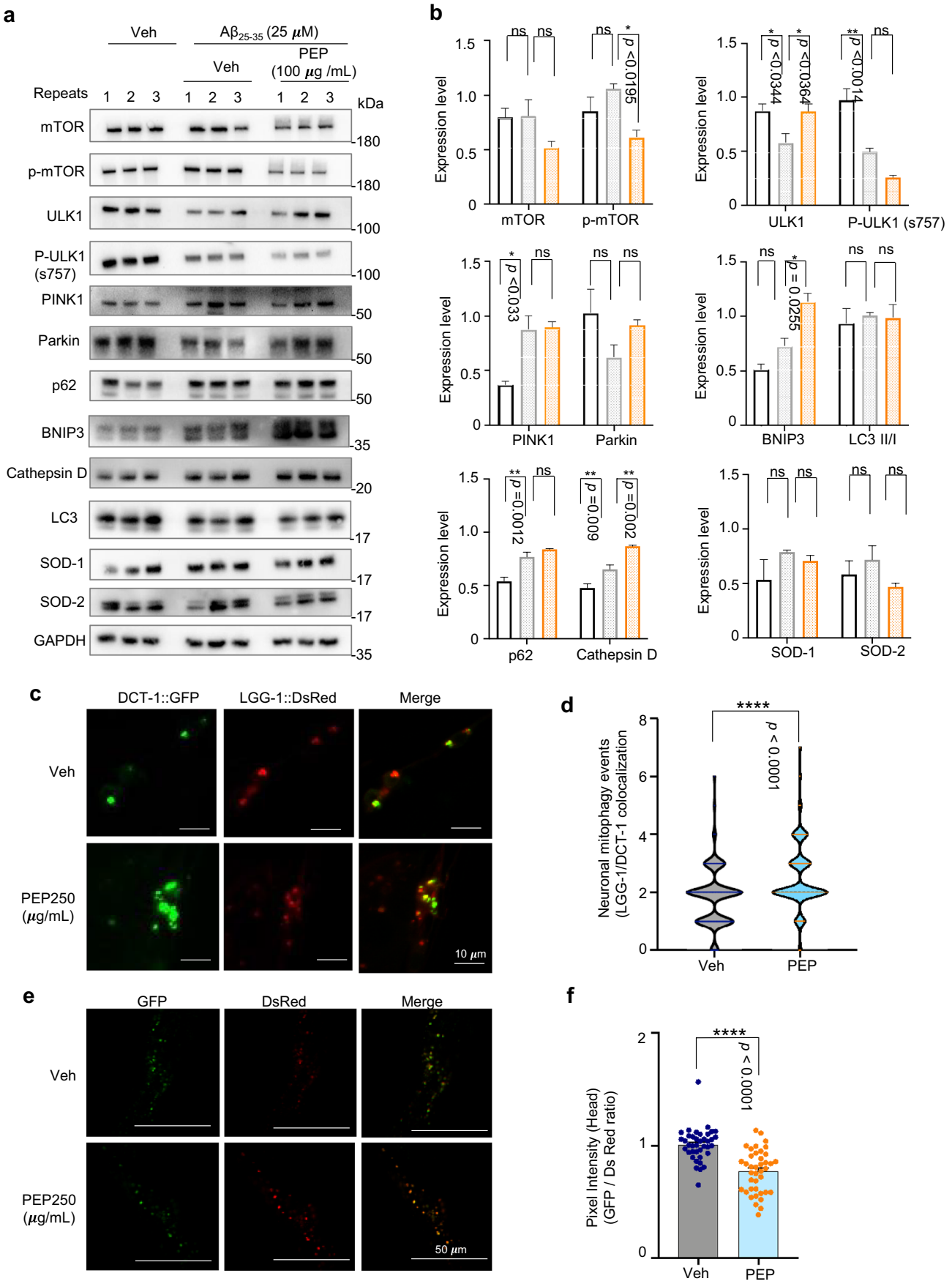
a
Veh
Aβ25-35 (25 μM)
Veh
PEP (100 μg /mL)
Repeats 1 2 3 1 2 3 1 2 3
kDa
mTOR
p-mTOR
ULK1
P-ULK1 (s757)
PINK1
Parkin
p62
BNIP3
Cathepsin D
LC3
SOD-1
SOD-2
GAPDH
180
180
100
100
50
50
50
35
20
17
17
17
35
b
Expression level
mTOR
p-mTOR
ULK1
P-ULK1 (s757)
PINK1
Parkin
BNIP3
LC3 II/I
p62
Cathepsin D
SOD-1
SOD-2
ns
p <0.0195
p <0.0344
p <0.0364
p <0.0014
p <0.033
p = 0.0255
p =0.0012
p =0.009
p =0.002
c
DCT-1::GFP
LGG-1::DsRed
Merge
Veh
PEP250 (μg/mL)
10 μm
d
Neuronal mitophagy events (LGG-1/DCT-1 colocalization)
****
p < 0.0001
Veh
PEP
e
GFP
DsRed
Merge
Veh
PEP250 (μg/mL)
50 μm
f
Pixel Intensity (Head) (GFP / Ds Red ratio)
****
p < 0.0001
Veh
PEP

◂**Fig. 4** PEP induced mitophagy in human SH-SY5Y-differentiated neuronal-like cells and *C. elegans* neurons. **a** Effects of $A\beta_{25\text{-}35}$ (25 μM) and PEP (100 μg/mL) on the expression of designated proteins in SH-SY5Y-differentiated neuronal-like cells. **b** Quantifications of the expression level of designated proteins as compared to GAPDH. Data were from three biological repeats. One-way ANOVA followed by Tukey's multiple comparisons test was used for data analysis with ns, no significance; $^{*}p<0.05$, $^{**}p<0.01$, $^{***}p<0.001$, $^{****}p<0.0001$. **c** Representative images showing the LGG-1 and DCT-1 co-localization in control or PEP (250 μg/mL) extract fed adult day 1 nematodes. Scale bar, 10 μm. **d** PEP enhanced LGG-1 and DCT-1 co-localization which indicate mitophagy events. Data were from two biological repeats with a total of 38 to 45 nematodes used for data quantification. One-way ANOVA followed by Tukey's multiple comparisons test was used for data analysis with ns, no significance; $^{*}p<0.05$, $^{**}p<0.01$, $^{***}p<0.001$, $^{****}p<0.0001$. **e** Representative images showing the GFP/DsRed ratio in control or PEP (250 μg/ml) extract fed adult day 1 mtRosella nematodes. Scale bar, 50 μm. **f** PEP reduced GFP/DsRed ratio indicating increased mitophagy. Data were from three biological repeats with 40 nematodes. One-way ANOVA followed by Tukey's multiple comparisons test was used for data analysis with ns, no significance; $^{*}p<0.05$, $^{**}p<0.01$, $^{***}p<0.001$, $^{****}p<0.0001$. Original western blot gels for **a** are included in Supplementary Fig. 2

list of potential candidates which might inhibit AD pathologies and own translational potential, we considered capacity of compound candidates to pass the blood–brain barrier (BBB) [53, 54]. We used the SwissADME software to predict BBB permeability of all compounds. As a result, 15 compounds were highly ranked with BBB permeability (Table 1). While the compound phenol showed the highest BBB permeability score in this system, others such as squalene, tocopherols, and amyrins may have high affinity to BBB receptor(s) in the BBB permeant system. Since PEP extract enhanced DAF-16 nuclear localization, a computer docking analysis was used to predict whether PEP extract containing potential compounds could induce FOXO3/DAF-16 nuclear translocation in different conditions, including via inhibiting the insulin/IGF-1 signaling pathway. 2KJI, an insulin-like protein found in *C. elegans*, was used as a target protein, and the docking analysis was performed on the top 10 potential compounds in the list. For the results, a higher negative binding energy indicates a higher stability of the protein–ligand complex. In our study (Supplementary Table 3), tocopherols including α-tocopherol (−8.556 kcal/mol), ϒ-tocopherol (−8.356 kcal/mol), and δ-tocopherol (−8.227 kcal/mol) showed the highest binding potential to the insulin-like protein in *C. elegans*. Other compounds such as stigmast-4-en-3-one (−8.246 kcal/mol), squalene (−8.186 kcal/mol), and cholest-4-en-3-one (−8.151 kcal/mol), α-amyrin (−7.874 kcal/mol), as well as β-amyrin (−7.453 kcal/mol) could form a stable complex with 2KJI; these data suggest that attenuation of the insulin pathway via these compounds may activate DAF-16 nuclear translocation. Further wet laboratory experiments are necessary to identify the compound(s) that could induce mitophagy and forestall memory loss and attenuate pathologies in AD animals.

Discussion and Conclusion

Where there is no drug available to cure AD, turning up mitophagy is suggested as a promising strategy for anti-AD drug development [10, 27, 55]. Here, we demonstrate that PEP extract inhibits $A\beta_{25\text{-}35}$-induced mitochondrial superoxide production and loss of MMP, which then attenuated neuronal cell death. PEP extract not only increases neuronal mitophagy level and alleviates neurodegeneration, but also inhibits memory impairment in AD *C. elegans*, especially in the $hA\beta_{1\text{-}42}$ model of AD. In particular, we show these benefits to be mediated by the nuclear localization of DAF-16, which stimulates mitophagy and protects against oxidative stress. FOXO3/DAF-16 is a fundamental component of the insulin/IGF signaling (IIS) pathway, which plays a critical role in longevity and stress resistance in various organisms including in humans [56–59]. In *C. elegans*, DAF-16 not only regulates longevity and dauer development, but is also involved in metabolism and stress resistance. The activity of DAF-16 is regulated by the upstream protein, DAF-2 (orthologue of the mammalian insulin and insulin-like growth factor-1 receptor) [60, 61]. Upon activation, DAF-16 disconnects from the 14–3-3 proteins that negatively regulates the insulin-like signaling (IIS) pathway and is positively regulated by the JNK pathway [62]. Upon translocation to the nucleus, DAF-16 promotes target gene expression of transmembrane tyrosine kinase (*old-1*) [63], glutathione-S-transferase 4 (*gst4*) [64, 65], BNIP3/NIX/*dct-1* [47, 66], and *sod-3* [67, 68]. Here, we show that the DAF-16-regulated downstream genes, including *gst-4* and *sod-3*, were increased upon PEP supplementation. Previous studies suggested that activated neuronal DAF-16 elicits intestinal DAF-16 activation, and vice versa [69, 70]. Here, our results showed that PEP increased DAF-16 nuclear translocation. In turn, activated DAF-16 directly promotes *sod-3* expression level. To note, although enhanced DAF-16 activity, we did not detect significant change of *dct-1*; this could be caused by the use of whole worm tissue for the PCR rather than to use the isolated neurons. Related experiments could be performed using a neuronal isolation protocol for tissue collection in the future. Interestingly, our immunoblot data show that PEP activated ULK1, an essential protein involved in both autophagy and mitophagy [43, 71], via inhibiting mTOR. Additionally, PEP increased the expression levels of BNIP3 (the mammalian homolog of the *C. elegans dct-1*) and the lysosome protein cathepsin D; upregulation of these mitophagy/lysosome proteins could enhance mitophagy. In line with this, two in vivo mitophagy quantification assays unambiguously support the possibility of a neuronal mitophagy induction capacity by PEP via the DAF-16/DCT-1/SOD3 pathway. Importantly, knocked

Revised Proof

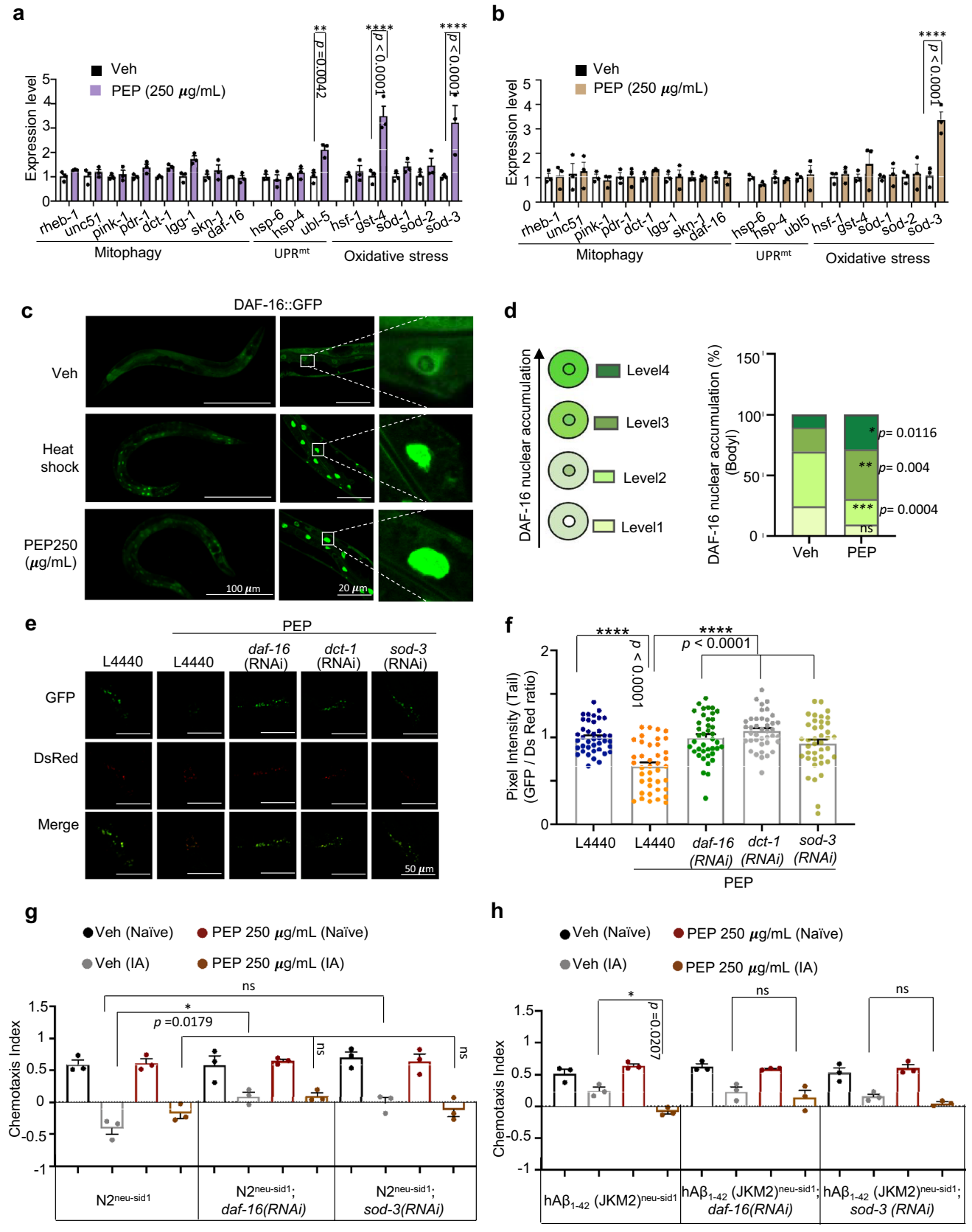
a
Veh
PEP (250 μg/mL)
Expression level
p =0.0042
p < 0.0001
p < 0.0001
rheb-1
unc51
pink-1
pdr-1
dct-1
lgg-1
skn-1
daf-16
hsp-6
hsp-4
ubl-5
hsf-1
gst-4
sod-1
sod-2
sod-3
Mitophagy
UPRmt
Oxidative stress
b
Veh
PEP (250 μg/mL)
Expression level
p < 0.0001
Mitophagy
UPRmt
Oxidative stress
c
DAF-16::GFP
Veh
Heat shock
PEP250 (μg/mL)
100 μm
20 μm
d
DAF-16 nuclear accumulation
Level4
Level3
Level2
Level1
DAF-16 nuclear accumulation (%) (Body)
p= 0.0116
p= 0.004
p= 0.0004
ns
Veh
PEP
e
PEP
L4440
L4440
daf-16 (RNAi)
dct-1 (RNAi)
sod-3 (RNAi)
GFP
DsRed
Merge
50 μm
f
Pixel Intensity (Tail) (GFP / Ds Red ratio)
p < 0.0001
p < 0.0001
L4440
L4440
daf-16 (RNAi)
dct-1 (RNAi)
sod-3 (RNAi)
PEP
g
Veh (Naïve)
PEP 250 μg/mL (Naïve)
Veh (IA)
PEP 250 μg/mL (IA)
Chemotaxis Index
p =0.0179
ns
ns
ns
N2neu-sid1
N2neu-sid1; daf-16(RNAi)
N2neu-sid1; sod-3(RNAi)
h
Veh (Naïve)
PEP 250 μg/mL (Naïve)
Veh (IA)
PEP 250 μg/mL (IA)
Chemotaxis Index
p =0.0207
ns
ns
hAβ1-42 (JKM2)neu-sid1
hAβ1-42 (JKM2)neu-sid1; daf-16(RNAi)
hAβ1-42 (JKM2)neu-sid1; sod-3 (RNAi)

◂**Fig. 5** PEP induces DAF-16 nuclear localization, leading to higher transcriptional regulation of downstream genes. **a**, **b** Effect of PEP on mitochondria-related gene expression in day 1 WT (N2) and $hA\beta_{1-42}$ (JKM2) nematodes. Data were from three biological repeats (each biological repeat includes three technical repeats). Two-way ANOVA followed by Sidak's multiple comparisons test was used for data analysis with ns, no significance, $*p<0.05$, $**p<0.01$, $***p<0.001$, $****p<0.0001$. **c** Images showing differential subcellular distribution of DAF-16 in vehicle (left), heat-shock (37 °C, 30 min, positive control) (middle), and PEP (250 µg/mL) nematodes (right). Scale bars, 100 µm and 20 µm, respectively. **d** PEP promoted DAF-16 nuclear translocation in adult day 1 nematodes. Nematodes were treated with PEP (250 µg/mL) from L4 stage. Data were from two biological repeats with 40 nematodes (each biological repeat includes three technical repeats). One-way ANOVA followed by Tukey's multiple comparisons test was used for data analysis with ns, no significance; $*p<0.05$, $**p<0.01$, $***p<0.001$. **e** Representative images showing effects of *daf-16*, *dct-1*, and *sod-3* on GFP/DsRed ratio in PEP (250 µg/mL) extract fed adult day 1 $mtRosella^{Neu-sid1}$ nematodes. Scale bar, 50 µm. **f** Knock down of neuronal *daf-16*, *dct-1*, and *sod-3* gene affected PEP-dependent neuronal mitophagy induction in $mtRosella^{Neu-sid1}$ nematodes. Data were from two to three biological repeats with the results from a total of 40 nematodes (each biological repeat includes three technical repeats). One-way ANOVA followed by Tukey's multiple comparisons test was used for data analysis with ns, no significance, $*p<0.05$, $**p<0.01$, $***p<0.001$, $****p<0.0001$. **g**, **h** Knock down of neuronal *daf-16* or *sod-3* gene affected PEP-induced memory improvement in the $N2^{neu-sid1}$ (**g**) and $hA\beta_{1-42}$ $(JKM2)^{neu-sid1}$ (**h**) nematodes. Data were from four biological repeats with the results shown in mean ± SEM. One-way ANOVA followed by Tukey's multiple comparisons test was used for data analysis with ns, no significance, $*p<0.05$, $**p<0.01$, $***p<0.001$, $****p<0.0001$

down *daf-16* or *sod-3* also annulled the memory benefits of PEP extract in $hA\beta_{1-42}$ AD-like animals. Taking all the pieces of data together, it suggests that PEP could regulate both mitophagy and mitochondrial resilience, which may contribute to memory retention and neuroprotection in the AD animals via DAF-16 dependent pathways (Fig. 6).

Until here, the neuroprotective effects and underlying mechanism of PEP extract have been partially uncovered in this study. By extrapolation, it is likely that multiple small compounds in PEP that contributed to the beneficial effects. Fortunately, our findings clearly show *P. edulis* pericarp could be a good source of bioactive compounds, and potential compounds of PEP extract were identified in this study. In the future, it will be interesting to continue studying the therapeutic ability of the potential candidates in multiple AD models.

Materials and Methods

Chemicals

Dulbecco's modified Eagle medium (DMEM), fetal bovine serum (FBS), penicillin–streptomycin, petroleum ether, retinoic acid (RA), thiazolyl blue tetrazolium bromide, and ampicillin were purchased from Sigma-Aldrich. DEME/F-12 (1:1) (1X) + GlutaMAX™-lDulbecco's modified Eagle medium F-12 nutrient mixture (Ham) was purchased from Gibco® by Life Technologies™. Dimethyl sulfoxide (DMSO), tetramethylrhodamine methyl ester perchlorate (TMRM), and isopropylthio-ß-galactoside (IPTG) were purchased from Merck. The CytoTox 96® LDH kit was purchased from Promega. β-$Amyloid_{25-35}$ and BDNF (human) were purchased from GenScript®. TRIzol reagent ® (Cat. #BCCD4264) was purchased from Sigma® Life Science. NuPAGE™ 4–12% Bis–Tris gels were purchased from Invitrogen by Thermo Fisher Scientific. MitoSOX™ Red mitochondrial superoxide indicator and Hoechst 33,342 solution were purchased from Thermo Fisher Scientific. *Power*SYBR® Green PCR master mix was purchased from Applied Biosystems by Thermo Fisher Scientific. NuPAGE® MES SDS Running Buffer (20X) and NuPAGE® Transfer Buffer (20X) were purchased from Invitrogen by Life Technologies™ and Nover® by Life Technologies™, respectively. Immun-Blot® PVDF membranes for protein blotting (Cat. #1620177) and iScript cDNA Synthesis kit (Cat. #1708891) were purchased from BIO-RAD. Additionally, nonfat dry milk, antibodies including mTOR (7C10), ULK1 (D9D7), p-ULK1 (ser757) (D7O6U), SQSTM1/p62 (#5114), Parkin [PRK8], BNIP3 (D7U1T), and GAPDH (14C10) as well as anti-rabbit IgG HRP-linked antibody and anti-mouse IgG HRP-linked antibody were purchased from Cell Signaling. Antibodies including p-mTOR (ab109286), pink1 (38CT18.7), SOD1 (ab13498), SOD2 [2A1] (ab16956), cathepsin D [CTD-19] (ab6313), and GAP43 (ab12274) were purchased from Abcam.

Plant Collection and Preparation

The fresh passion fruit (*P. edulis* 'Paul Ecke') was collected from Chiang Mai, Thailand, and identified by the herbarium of Kasin Suvatabhandju (Department of Botany, Faculty of Science, Chulalongkorn University, Thailand) with the voucher specimen [016437 B(CU)]. Pericarp was cut and air-dried before being ground into a fine powder. *P. edulis* pericarp powder was macerated in petroleum ether with a ratio of 1:10. The PEP extract was filtered through Whatman No. 1 filter paper and concentrated using vacuum distillation and a rotary evaporator. Stock solution was prepared in DMSO (concentration is 100 mg/ml).

Cell Culture

HT-22, a mouse hippocampal cell (a gift from Professor David Schubert, San Diego, CA, USA), were cultured and maintained in DMEM with 10% FBS supplementary and 1% penicillin–streptomycin. SHSY5Y, a human fibroblastoma cells were cultured and maintained in DMEM/F12 with 10%

Revised Proof

Table 1 The SwissADME software was used for in silico prediction of BBB permeability of a list of compounds identified in the *P. edulis* pericarp extract

Numbers	Name	Predicted as BBB permeant
1	Phenol	Yes
2	Squalene	No
3	γ-Tocopherol	No
4	α-Tocopherol	No
5	β-Amyrin	No
6	δ-Tocopherol	No
7	α-Amyrin	No
8	Cholest-4-en-3-one	No
9	α-Spinasterone	No
10	Stigmast-4-en-3-one	No
11	Phytol	No
12	Behenic alcohol	No
13	α-Tocopherolquinone	No
14	9,19-Cyclolanost-7-en-3-ol	No
15	9,19-Cyclolanostane-3,7-diol	No

FBS supplementary and 1% penicillin–streptomycin (normal culture medium). Cells were maintained in a humidified incubator (37 °C, 5% CO_2). Culture medium was changed every 2 to 3 days and 80 to 90% confluence cells were used for future experiments.

Cell Differentiation

SH-SY5Y cell differentiation was induced using a previously described protocol with slight modifications [72]. Briefly, at day 0, SHSY5Y cells were seeded into the experimental plates with normal culture medium and cultured overnight. On day 1, we replace the normal culture medium by using DMEM/F12 medium (5% FBS) with retinoic acid (RA) (10 µM) to initiate cell differentiation, and change to DMEM/F12 medium (2.5% FBS) with RA (10 µM) to stimulate further cell differentiation in day 2 to day 5. Additionally, DMEM/F12 medium (0% FBS) with 50 ng/mL brain-derived neurotrophic factor (BDNF) was used to strengthening cell differentiation in day 6 to day 8. Then, the differentiated cells are ready for experiments on day 9.

Cell Viability

3-(4,5-Dimethylthiazol-2-yl)-2,5-diphenyl tetrazolium bromide (MTT) is a widely used chemical indicator for cellular metabolic activity and cell viability based on the ability of nicotinamide adenine dinucleotide phosphate (NADPH)–dependent cellular oxidoreductase enzymes which reduce the yellow MTT to purple formazan in living cells. The formazan redissolved in the solubilization solution such as DMSO and provides a colorimetric assay. In this study, MTT was used to detect cell viability for both HT-22 and SHSY5Y cells. For HT-22 cells, 5000 cells were seeded and grown in each well of 96-well plates overnight in a humidified 5% CO_2 incubator at 37 °C. Next day, the cells were pretreated (6 h, 12 h) or co-treated with varied concentrations of PEP extract (12.5 to 100 µg/mL) and glutamate (5 mM). At the end of the drug treatment time, cells were exposed to MTT for 3 h. Then, all supernatant was removed, and the formazan crystals were dissolved with DMSO (200 µL) before measuring the absorbance at 550 nm. For SHSY5Y cells, the differentiated cells were used for cell viability detection. As mentioned earlier, cells are ready to use after a 9-day differentiation period, and pretreated (6 h, 12 h) or co-treated with varied concentrations of PEP extract (12.5 to 100 µg/mL) and $Aß_{25-35}$ (25 µM). At the end of the drug treatment time, cells were exposed to MTT for 3 h. Then, the synthesized formazan crystals were dissolved with DMSO (200 µL) before measuring the absorbance at 550 nm.

Detection of Mitochondrial Superoxide in Live Cells

MitoSOX™ Red is a cell permeant dye that selectively targets mitochondria. Neuronal differentiated SH-SY5Y cells were pretreated (6 h ahead) or co-treated with PEP extract (100 µg/mL) and $Aß_{25-35}$ (25 µM). Antimycin A1 (30 min, 100 µM) was used as a positive control. After designated time of treatment, cells were stained with MitoSOX™ Red reagent (4 µM) for 10 min in the dark. The cells were washed with warm 1 × PBS once and imaged using a confocal microscope at 40 × magnification.

Detection of Mitochondrial Membrane Potential in Live Cells

TMRM is a cell permeant mitochondrial membrane potential indicator that accumulates in live mitochondria showing bright fluorescent signal. Neuronal differentiated SH-SY5Y cells were pretreated (6 h ahead) or co-treated with PEP extract (100 µg/mL) and $Aß_{25-35}$ (25 µM). FCCP (1 h, 20 µM) was used as a positive control. After designated time of treatment, cells were stained with TMRM (150 nM) and Hoechst 33342 (2 µg/mL) for 30 min in the dark. The cells were washed with warm medium and imaged using a confocal microscope at 40 × magnification.

Gas Chromatography-Mass Spectrometry (GC–MS) and Theoretical Prediction of Blood–Brain Barrier (BBB) Permeability of Compounds Analysis

The beneficial effects of the PEP extract are due to the various potential compounds. GC–MS was employed to

Revised Proof

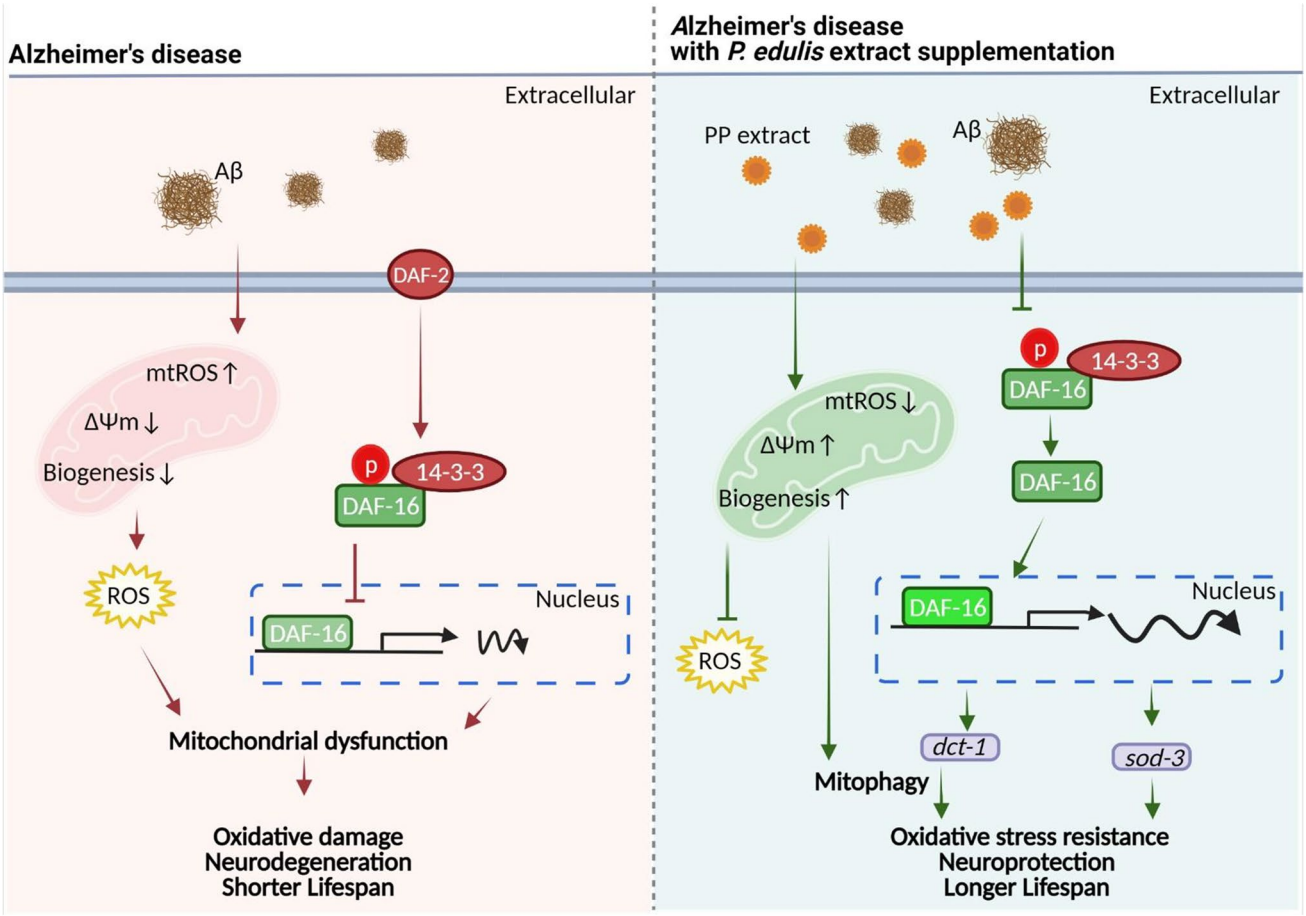

Fig. 6 PEP protects against Aβ-induced neurotoxicity via the DAF-16 pathway. Aβ limited activation of DAF-16, induced production of mitochondrial superoxide, and caused mitochondrial dysfunction, which promotes the progression of AD. However, PEP administration maintained mitochondrial homeostasis and increased mitophagy levels via the DAF-16 pathway, which attenuates Aβ-induced toxicity in AD models

uncover the potential drug candidates in PEP extract. PEP subfractions were sent to Scientific and Technological Research Equipment Center (STREC), Chulalongkorn University, Thailand, for GC–MS analysis by using the Agilent 7890B GC system coupled with a HP-5 ms (part no. 19091S-433UI (30 m × 0.25 mm, 0.25 µm)) capillary column. The extracts were dissolved in hexane, and 1 µl was injected into the column for analysis with a total of 68-min run time. Results were analyzed using MassHunter 2014 software and the potential compounds were identified by comparing with the spectral patterns with the National Institute of Standards and Technology (NIST) 2011 library. To further narrow down the potential compounds, SwissADME software (http://www.swissadme.ch) was used to analyze the BBB permeability of identified compounds, and DockThor (https://dockthor.lncc.br/v2/), an online software, was used for docking analysis.

Western Blot

Cell samples were collected by using 1 × radioimmunoprecipitation assay (RIPA) buffer with protease inhibitors and phosphatase inhibitors. Protein samples were running on an NuPAGE 4–12% Bis–Tris protein gel. The chemiluminescence reaction was detected using a ChemiDoc XRS System (Bio-Rad Laboratories). The following antibodies were used in this study: mTOR, p-mTOR, ULK1, p-ULK1(s757), pink1, Parkin, p62, BNIP3, cathepsin D, LC3B, SOD1, SOD2, GAP43, and GAPDH.

C. elegans Strains

C. elegans strains were maintained on *Escherichia coli* OP50 using the standard feeding methods. The temperature for

rearing *C. elegans* was kept at 20 °C. The list of strains used in this study is shown in Supplementary Table 3.

Drug Treatment of *C. elegans*

The PEP extract or equal volume of DMSO was directly added in the melted NGM before being poured into the plates. Nematodes were treated from either egg hatching or L4 stage.

Toxicity Assay

A toxicity assay was used to determine the safe dose of PEP extract selection in *C. elegans*. N2, a wild-type strain, was used for these experiments. At day 1, ten of 1-day-old nematodes were placed on the NGM plates with OP50 which contained PEP extract (0.025, 0.25, 0.5 mg/mL) or not (vehicle) for 3-h egg laying. The number of eggs was counted after adults were removed. On day 2, the number of L1 larvae and unhatched eggs was counted to check the egg hatching efficiency. In day 3, the number of L4 larvae was counted. On day 4, the number of 1-day-old adult nematodes was counted. Each group includes three technical repeats.

Lifespan and Healthy Span Analysis

AD caused health issues and reduction of lifespan has been reported [1, 73]. We recorded the living time to check whether PEP extract have beneficial effects for lifespan extension in healthy (N2) nematodes and AD human Tau[P301L] and human $A\beta_{1\text{-}42}$ transgenic nematodes. The animals were synchronized by bleaching and grown at 20 °C until the L4 stage. Twenty of L4 stage animals were picked and placed in each experiment plate (with or without PEP extract). FUDR was added to prevent egg hatching and animals were transferred to the fresh plates for every 2–3 days until day 10, and then every 5–6 days (if food running out) until death. The number of living or dead animals was recorded every day until the last animal's death. Every experiment included 3 technical repeats. Additionally, *C. elegans* drawing food through its pharynx and the times of pharyngeal contraction and relaxation indicate the food uptake rate. Along with the lifespan experiment, the pharyngeal pumping rate of day 2 and day 8 nematodes was evaluated via manually counting for 30 s, and 10 animals were randomly selected from each technical repeat.

Chemotaxis Behavior Assay

Isoamyl alcohol (IA), a volatile liquid, was employed to perform the chemotaxis assay as previously described [74, 75]. Briefly, animals were synchronized by bleaching and grown on the OP50 seeded NGM plates with or without PEP extract at 20 °C until day 1. Animals (200 to 300 nematodes/group) were collected and washed 4 times with MilliQ water, and then placed on conditional NGM plates (no OP50) with/without IA on the middle of lid (10 µL) for 90 min. After that, animals were washed and transferred to the start point in the experimental plates and the number of animals from each area was recorded after 2 h. The experimental plate (10 cm) is separated into three main areas, which were labeled as IA, T (trap point), and S (start point). A small piece of Parafilm was placed in the middle of the "IA" area and 3 µl of 2% IA was topped on the Parafilm. The chemotaxis index was calculated as ("IA" – "T") / ("IA" + "T" + "S").

mRNA Quantification in *C. elegans* Tissue

Target gene expression in *C. elegans* was determined using real-time PCR. Animals were synchronized by bleaching and grown on the OP50 seeded NGM plates with or without PEP extract at 20 °C until adult day 1. Nematodes were collected, and then total RNA was further isolated using TRIzol™ reagent. The concentration of RNA was detected using a NanoDrop machine under absorbance 260 nm. cDNA samples were prepared using the iScript™ cDNA synthesis kit, and synthesis for 5 min at 25 °C, 20 min at 46 °C, 1 min at 95 °C, and finishing at 4 °C. The synthesized cDNA samples were used for real-time quantitative reverse transcription PCR (RT-qPCR) for target gene expression quantification. A total of nine samples for three biological repeats (three technical repeats for each biological repeat) were used. *Power*SYBR® Green PCR Master Mix was employed for quantitative PCR analysis. For each reaction, 4 µl of cDNA temple was mixed with 2 × *Power*SYBR® Green PCR Master Mix (5 µL), forward primer (0.5 µL), reverse primer (0.5 µL) in total 10 µL. Real-time qPCR reactions were performed in QuantStudio™ 7 Flex System v1.1 (Applied Biosystems by Life Technologies). The thermal cycling condition was set as pre-denaturation step at 95 ℃ for 10 min, which is followed by 40 cycles of denaturation at 95 ℃ for 15 s, annealing at 60 ℃ for 1 min, and extension at 95 ℃ for 15 s and 60℃ for 1 min. A melting curve was performed to confirm product formation. Data was calculated by using the $2^{-\Delta\Delta CT}$ method. The primers used in this study are listed as follows:

rheh-1, 5′-GGCTCCAACCTTACCACTCC-3′ and 5′-GCAAATCCTACT GCTGCTCC-3′,
unc-51, 5′-CTACACGTGGTGACTCTCCG-3′ and 5′-ATGCAATACGACGCGAAAGC-3′
pink-1,5′-AGCATATCGAATCGCAAATGAGTTAG-3′ and 5′-TCGACCGTGGCGAGTTACAAG-3′,
pdr-1, 5′-AGCCACCGAGCGATTGATTGC-3′ and 5′-GTGGCATTTTGGGCATCTTCTTG-3′,
dct-1, 5′-GGCTCCAACCTTACCACTCC-3′ and 5′-GCA AATCCTACT GCTGCTCC-3′,

Revised Proof

lgg-1, 5′-ACATGATTTTCTGGGAGGGG-3′ and 5′-TCTAATGGAAACCCAAAGCC-3′,
skn-1, 5′-ACAGTGCTTCTCTTCGGTAGC-3′ and 5′-GAGACCCATTGGACGGTTGA-3′,
daf-16, 5′-AAGCCGATTAAGACGGAACC-3′ and 5′-GTAGTGGCATTGGCTTGAAG-3′,
hsp-6, 5′-AACCACCGTCAACAACGCCG-3′ and 5′-AGCGATGATCTTATCTCCAGCGTCC-3′,
hsp-4, 5′-GCACTGGCCGTTCAAGATCGTCG-3′ and 5′-TGCTGGCACGGTGACAACGG-3′,
ubl-5, 5′-ACAAACTGGAACACGATGGGA-3′ and 5′-TCCCTCGTGAATCTCGTAATCC-3′,
hsf-1, 5′-GAATGCGACTAGGCAAATGGC-3′ and 5′-GGTGGATGAGGTGGAAGTCG-3′,
gst-4, 5′-TGCTCTTGCTGAGCCAATCCGT-3′ and 5′-CCAGCGAGTCCAAATTTTCTTGCCA-3′,
sod-1, 5′-CCGACACGCTCGTCACGCTT-3′ and 5′-ACTGGGGAGCAGCGAGAGCA-3′,
sod-2, 5′-ACAGGAGTCGCTGCTGTTCGC-3′ and 5′-TCCTTTGGAGACCGCCTCGTGA-3′,
sod-3, 5′-CTAAGGATGGTGAACCTTCA-3′ and 5′-CGCGCTTAATAGTGTCCATCAG-3′,
pmp-3, 5′-ATGATAAATCAGCGTCCCGAC-3′ and 5′-TTGCAACGAGAGCAACTGAAC-3′.

Aldicarb Assay

Aldicarb, an acetylcholinesterase inhibitor, was employed to evaluate the sensitivity of *C. elegans* to the synaptic transmission of acetylcholine at the neuromuscular junction. The *C. elegans* strains VC233 and NM204 grown on the OP50 seeded NGM plates were used as hypersensitive and resistant control in the experiment, respectively. Animals for experiments were synchronized by bleaching and grown on the OP50 seeded NGM plates with or without PEP extract at 20 °C until day 1. Thirty animals were transferred on each NGM plate with 0.75 mM aldicarb, and the non-paralyzed animals were recorded every 30 min for the aldicarb-induced paralysis. Each experimental group includes 3 biological repeats and 3 technical repeats.

Glutamatergic Neurons Imaging

Glutamatergic neurodegeneration was detected in *C. elegans* using the previous reported method. Animals were synchronized by bleaching and grown on the OP50 seeded NGM plates with or without PEP extract at 20 °C until adult day 3. There are about 15 glutamatergic neurons in the worm tail region, and 5 were selected in this study, which are LUA(R), LUA(L), PVR, PLM(R), and PLM(L). The tail regions of day 3 animals were imaged using a confocal microscope. Each experimental group includes 2 biological repeats and 3 technical repeats.

Screening of Neuronal Mitophagy in *C. elegans*

Two *C. elegans* strains were employed to quantify mitophagy induction potential of PEP extract in *C. elegans*. For both experiments, the nematodes were prepared and placed on the OP50 seeded NGM plates with or without PEP extract (250 μg/ml) from the egg hatching stage. The first transgenic animal expressing LGG-1::DsRed (autophagosomal marker), together with DCT-1::GFP (mitophagy reporter) in neurons. The double positive animals (adult day 1) were paralyzed by levamisole, mounted on 4% agarose pads, and imaged using confocal microscopy. The co-localization of LGG-1 and DCT-1 was count for mitophagy events. Another transgenic animal expressing pan-neuronal mitophagy reporter (mt-Rosella biosensor) represents the mitophagy level according to the ratio between pH-sensitive GFP to pH-insensitive DsRed (the lower the ratio, the higher the mitophagy events). Day 1 animals were paralyzed by levamisole, mounted on 4% agarose pads, and imaged using a confocal microscope at 10 × or 40 × magnification. Each experimental group includes 2 to 3 biological repeats and 3 technical repeats.

DAF-16 Nuclear Localization

Animals were synchronized by bleaching and grown on the OP50 seeded NGM plates at 20 °C until L4 stage. Animals were transferred to the OP50 seeded NGM plates with or without PEP extract for 24 h. The DAF-16::GFP nuclear translocation of the adult day 1 nematodes was paralyzed by levamisole, mounted on 4% agarose pads, and imaged using a confocal microscope at 40 × magnification. Each experimental group includes 2 biological repeats and 2 technical repeats. The nuclear localization level was scored as level 1 to level 4.

RNA Interference (RNAi) by Feeding

Feeding bacteria expressing dsRNA (feeding RNAi) was used to knock down selected targets (*daf-16* and *sod-3*) in *C. elegans*. Briefly, selected bacteria were grown in the LB (50 mg/mL ampicillin) and added on the NGM plates containing 1% ampicillin and 1% IPTG with/without PEP extract. The animals were synchronized by bleaching or egg laying and grown on these RNAi plates until adult day 1 for chemotaxis behavior experiments and neuronal mitophagy screening assay, respectively.

Statistical Analysis

All results presented in this study have at least two biological repeats, except lifespan (one biological repeat with three technical repeats). For the imaging base experiments, data

Revised Proof

were quantified using ImageJ software. And statistical data was analyzed using Prism 8.0 software. The data were presented in mean ± SEM. The difference between the two treatment groups was analyzed using unpaired *t*-tests. And the group differences were analyzed using one-way ANOVA with Tukey's multiple comparisons test. The difference for multiple targets was analysis using two-way ANOVA with Sidak's multiple comparisons test. $P < 0.05$ is considered as statistically significant.

Supplementary Information The online version contains supplementary material available at https://doi.org/10.1007/s12035-022-02904-5.

Acknowledgements We would like to thank Thale Dawn Patrick-Brown for the English language editing.

Author Contribution T.T. and E.F.F. conceptualized and supervised the study. E.F.F. managed the research project, provided resources, as well as evaluated methodologies for the study. S.Q.C. and Y.A. performed the experiments and data analysis. T.T. and E.F.F. validated the experimental results. S.Q.C. and Y.A. wrote the first draft of the manuscript. T.T. and E.F.F. revised the manuscript, and all approved the final manuscript.

Funding S.Q.C. is a Ph.D. student in Clinical Biochemistry and Molecular Medicine, Department of Clinical Chemistry, Faculty of Allied Health Sciences, Chulalongkorn University, Thailand, and a visiting Ph.D. student in the Department of Clinical Molecular Biology, University of Oslo and Akershus University Hospital Norway. Her study was financially supported by the scholarship from the Graduate School, Chulalongkorn University to commemorate 72nd Anniversary of his Majesty King Bhumibol Adulyadej and the 100th Anniversary Chulalongkorn University Fund for Doctoral Scholarship as well as the 90th Anniversary Chulalongkorn University Fund (Ratchadaphiseksomphot Endowment Fund) and Overseas Research Experience scholarship for Graduate student. E.F.F. was supported by HELSE SØR-ØST (#2017056, #2020001, #2021021), the Research Council of Norway (#262175), the National Natural Science Foundation of China (#81971327), Akershus University Hospital (#269901, #261973), the Civitan Norges Forskningsfond for Alzheimers sykdom (#281931), the Czech Republic-Norway KAPEPA programme (with Martin Vyhnálek, #TO01000215), and the Rosa sløyfe/Norwegian Cancer Society & Norwegian Breast Cancer Society (#207819).

Data Availability All data are in the manuscript and the associated supporting information file.

Declarations

Ethics Approval No ethical approval is required in the present manuscript.

Consent to Participate Not applicable.

Consent for Publication Not applicable.

Conflict of Interest S.Q.C., Y.A., and T.T. have no conflict of interests involved. E.F.F. has a CRADA arrangement with ChromaDex (USA) and is consultant to Aladdin Healthcare Technologies (UK and Germany), the Vancouver Dementia Prevention Centre (Canada), Intellectual Labs (Norway), and MindRank AI (China).

References

1. Wiley J (2021) Alzheimer's disease facts and figures. Alzheimers Dement 17:327–406
2. Kumar A, Sidhu J, Goyal A, Tsao JW, Svercauski J (2021) Alzheimer disease (nursing)
3. Alonso AD, Grundke-Iqbal I, Iqbal K (1996) Alzheimer's disease hyperphosphorylated tau sequesters normal tau into tangles of filaments and disassembles microtubules. Nat Med 2(7):783–787
4. Chen G et al (2000) A learning deficit related to age and β-amyloid plaques in a mouse model of Alzheimer's disease. Nature 408(6815):975–979
5. Goedert M et al (1989) Multiple isoforms of human microtubule-associated protein tau: sequences and localization in neurofibrillary tangles of Alzheimer's disease. Neuron 3(4):519–526
6. Hardy JA, Higgins GA (1992) Alzheimer's disease: the amyloid cascade hypothesis. Science 256(5054):184–186
7. Zhang Y, Zhang Y, Aman Y, Ng CT, Chau WH, Zhang Z, Yue M, Bohm C, Jia Y, Li S, Yuan Q (2021) Amyloid-β toxicity modulates tau phosphorylation through the PAX6 signalling pathway. Brain 144(9):2759–2770
8. Kobro-Flatmoen A et al (2021) Re-emphasizing early Alzheimer's disease pathology starting in select entorhinal neurons, with a special focus on mitophagy. Ageing Res Rev 67:101307
9. Kerr JS et al (2017) Mitophagy and Alzheimer's disease: cellular and molecular mechanisms. Trends Neurosci 40(3):151–166
10. Fang EF et al (2019) Mitophagy inhibits amyloid-beta and tau pathology and reverses cognitive deficits in models of Alzheimer's disease. Nat Neurosci 22(3):401–412
11. Canter RG, Penney J, Tsai LH (2016) The road to restoring neural circuits for the treatment of Alzheimer's disease. Nature 539(7628):187–196
12. Zhao N et al (2020) Alzheimer's risk factors age, APOE genotype, and sex drive distinct molecular pathways. Neuron 106(5):727–74.e6
13. Xu C et al (2021) TNF-alpha-dependent neuronal necroptosis regulated in Alzheimer's disease by coordination of RIPK1-p62 complex with autophagic UVRAG. Theranostics 11(19):9452–9469
14. Aguillón-Osma J et al (2019) Impact of in vitro gastrointestinal digestion on the bioaccessibility and antioxidant capacity of bioactive compounds from passion fruit (Passiflora edulis) leaves and juice extracts. J Food Biochem 43(7):e12879
15. Hu Y et al (2018) A new C-glycosyl flavone and a new neolignan glycoside from Passiflora edulis Sims peel. Nat Prod Res 32(19):2312–2318
16. Pereira DTV et al (2021) Integration of pressurized liquids and ultrasound in the extraction of bioactive compounds from passion fruit rinds: impact on phenolic yield, extraction kinetics and technical-economic evaluation. Innov Food Sci Emerg Technol 67:102549
17. Parliment TH (1972) Volatile constituents of passion fruit. J Agric Food Chem 20(5):1043–1045
18. Leão KM et al (2014) Odor potency, aroma profile and volatiles composition of cold pressed oil from industrial passion fruit residues. Ind Crops Prod 58:280–286
19. de Albuquerque MAC, Levit R, Beres C, Bedani R, de LeBlanc ADM, Saad SMI, LeBlanc JG (2019) Tropical fruit by-products water extracts as sources of soluble fibres and phenolic compounds with potential antioxidant, anti-inflammatory, and functional properties. J Funct Foods 52:724–733
20. do Carmo MCL et al (2020) Passion fruit (Passiflora edulis) leaf aqueous extract ameliorates intestinal epithelial barrier

Revised Proof

dysfunction and reverts inflammatory parameters in Caco-2 cells monolayer. Food Res Int 133:109162
21. Lourith N, Kanlayavattanakul M (2020) Passion fruit seed: its antioxidative extracts and potency in protection of skin aging, in Aging, Elsevier. p. 283-288
22. Nerdy N, Ritarwan K (2019) Hepatoprotective activity and nephroprotective activity of peel extract from three varieties of the passion fruit (Passiflora sp.) in the albino rat. Open Access Maced J Med Sci 7(4):536
23. Tal Y et al (2016) The neuroprotective properties of a novel variety of passion fruit. J Funct Foods 23:359–369
24. Dos Santos KC et al (2016) Passiflora actinia hydroalcoholic extract and its major constituent, isovitexin, are neuroprotective against glutamate-induced cell damage in mice hippocampal slices. J Pharm Pharmacol 68(2):282–291
25. Doungue HT, Kengne APN, Kuate D (2018) Neuroprotective effect and antioxidant activity of Passiflora edulis fruit flavonoid fraction, aqueous extract, and juice in aluminum chloride-induced Alzheimer's disease rats. Nutrire 43(1):1–12
26. Perry RJ, Watson P, Hodges JR (2000) The nature and staging of attention dysfunction in early (minimal and mild) Alzheimer's disease: relationship to episodic and semantic memory impairment. Neuropsychologia 38(3):252–271
27. Xie C, Zhuang XX, Niu Z, Ai R, Lautrup S, Zheng S, Jiang Y, Han R, Gupta TS, Cao S, Lagartos-Donate MJ (2022) Amelioration of Alzheimer's disease pathology by mitophagy inducers identified via machine learning and a cross-species workflow. Nature Biomedical Engineering 1–18
28. Gallrein C et al (2021) Novel amyloid-beta pathology C elegans model reveals distinct neurons as seeds of pathogenicity. Prog Neurobiol 198:101907
29. Cummins N, Tweedie A, Zuryn S, Bertran-Gonzalez J, Götz J (2019) Disease-associated tau impairs mitophagy by inhibiting Parkin translocation to mitochondria. EMBO J 38(3):e99360
30. Ping Y et al (2015) Linking aβ42-induced hyperexcitability to neurodegeneration, learning and motor deficits, and a shorter lifespan in an Alzheimer's model. PLoS Genet 11(3):e1005025
31. Dement A (2016) Alzheimer's disease facts and figures. Alzheimers Dement J Alzheimer Assoc 12(4):459–509
32. Cacabelos R, Takeda M, Winblad B (1999) The glutamatergic system and neurodegeneration in dementia: preventive strategies in Alzheimer's disease. International journal of geriatric psychiatry
33. Schliebs R, Arendt T (2006) The significance of the cholinergic system in the brain during aging and in Alzheimer's disease. J Neural Transm 113(11):1625–1644
34. Ferreira-Vieira TH et al (2016) Alzheimer's disease: targeting the cholinergic system. Curr Neuropharmacol 14(1):101–115
35. Gibson GE, Peterson C, Jenden DJ (1981) Brain acetylcholine synthesis declines with senescence. Science 213(4508):674–676
36. Singla N, Dhawan D (2017) Zinc improves cognitive and neuronal dysfunction during aluminium-induced neurodegeneration. Mol Neurobiol 54(1):406–422
37. Hampel H et al (2018) The cholinergic system in the pathophysiology and treatment of Alzheimer's disease. Brain 141(7):1917–1933
38. Mahoney TR, Luo S, Nonet ML (2006) Analysis of synaptic transmission in Caenorhabditis elegans using an aldicarb-sensitivity assay. Nat Protoc 1(4):1772–1777
39. Masliah E et al (1996) Deficient glutamate tranport is associated with neurodegeneration in Alzheimer's disease. Ann Neurol Off J Am Neurol Assoc Child Neurol Soc 40(5):759–766
40. Myhrer T (1998) Adverse psychological impact, glutamatergic dysfunction, and risk factors for Alzheimer's disease. Neurosci Biobehav Rev 23(1):131–139
41. Tu S et al (2014) Oligomeric Aβ-induced synaptic dysfunction in Alzheimer's disease. Mol Neurodegener 9(1):1–12
42. Griffin EF, Scopel SE, Stephen CA, Holzhauer AC, Vaji MA, Tuckey RA, Berkowitz LA, Caldwell KA, Caldwell GA (2019) ApoE-associated modulation of neuroprotection from Aβ mediated neurodegeneration in transgenic Caenorhabditis elegans. Dis Model Mech 12(2):dmm037218
43. Aman Y et al (2021) Autophagy in healthy ageing and disease. Nat Aging 1:634–650
44. Munson MJ et al (2021) GAK and PRKCD are positive regulators of PRKN-independent mitophagy. Nat Commun 12(1):6101
45. Fang EF et al (2019) Mitophagy inhibits amyloid-β and tau pathology and reverses cognitive deficits in models of Alzheimer's disease. Nat Neurosci 22(3):401–412
46. Fang EF, Palikaras K, Sun N, Fivenson EM, Spangler RD, Kerr JS, Cordonnier SA, Hou Y, Dombi E, Kassahun H, Tavernarakis N (2017) In vitro and in vivo detection of mitophagy in human cells, C. elegans, and mice. J Vis Exp JoVE (129):e56301
47. Palikaras K, Lionaki E, Tavernarakis N (2015) Coordination of mitophagy and mitochondrial biogenesis during ageing in C. elegans. Nature 521(7553):525–8
48. Mouchiroud L et al (2013) The NAD(+)/sirtuin pathway modulates longevity through activation of mitochondrial UPR and FOXO signaling. Cell 154(2):430–441
49. Fang EF et al (2014) Defective mitophagy in XPA via PARP-1 hyperactivation and NAD(+)/SIRT1 reduction. Cell 157(4):882–896
50. Ray A et al (2014) Mitochondrial dysfunction, oxidative stress, and neurodegeneration elicited by a bacterial metabolite in a C. elegans Parkinson's model. Cell Death Dis 5(1):e984–e984
51. Evans EA, Kawli T, Tan M-W (2008) Pseudomonas aeruginosa suppresses host immunity by activating the DAF-2 insulin-like signaling pathway in Caenorhabditis elegans. PLoS Pathog 4(10):e1000175
52. Henderson ST, Bonafe M, Johnson TE (2006) daf-16 protects the nematode Caenorhabditis elegans during food deprivation. J Gerontol A Biol Sci Med Sci 61(5):444–460
53. Van Tellingen O et al (2015) Overcoming the blood–brain tumor barrier for effective glioblastoma treatment. Drug Resist Updat 19:1–12
54. Pardridge WM (2015) Blood–brain barrier endogenous transporters as therapeutic targets: a new model for small molecule CNS drug discovery. Expert Opin Ther Targets 19(8):1059–1072
55. Kingwell K (2019) Turning up mitophagy in Alzheimer disease. Nat Rev Drug Discov
56. Barbieri M et al (2003) Insulin/IGF-I-signaling pathway: an evolutionarily conserved mechanism of longevity from yeast to humans. Am J Physiol-Endocrinol Metab 285(5):E1064–E1071
57. Willcox BJ et al (2008) FOXO3A genotype is strongly associated with human longevity. Proc Natl Acad Sci U S A 105(37):13987–13992
58. Murphy CT et al (2003) Genes that act downstream of DAF-16 to influence the lifespan of Caenorhabditis elegans. Nature 424(6946):277–283
59. Kaletsky R et al (2016) The C. elegans adult neuronal IIS/FOXO transcriptome reveals adult phenotype regulators. Nature 529(7584):92–6
60. Henderson ST, Johnson TE (2001) daf-16 integrates developmental and environmental inputs to mediate aging in the nematode Caenorhabditis elegans. Curr Biol 11(24):1975–1980
61. Kenyon C et al (1993) A C. elegans mutant that lives twice as long as wild type. Nature 366(6454):461–4
62. Oh SW et al (2005) JNK regulates lifespan in Caenorhabditis elegans by modulating nuclear translocation of forkhead transcription factor/DAF-16. Proc Natl Acad Sci 102(12):4494–4499

Revised Proof

63. Murakami S, Johnson TE (2001) The OLD-1 positive regulator of longevity and stress resistance is under DAF-16 regulation in Caenorhabditis elegans. Curr Biol 11(19):1517–1523
64. Shanmugam G et al (2017) Diosgenin a phytosterol substitute for cholesterol, prolongs the lifespan and mitigates glucose toxicity via DAF-16/FOXO and GST-4 in Caenorhabditis elegans. Biomed Pharmacother 95:1693–1703
65. Zhang L, Gu B, Wang Y (2021) Clove essential oil confers antioxidant activity and lifespan extension in C. elegans via the DAF-16/FOXO transcription factor. Comp Biochem Physiol C Toxicol Pharmacol 242:108938
66. Fang EF et al (2016) NAD(+) replenishment improves lifespan and healthspan in ataxia telangiectasia models via mitophagy and DNA Repair. Cell Metab 24(4):566–581
67. Honda Y, Honda S (1999) The daf-2 gene network for longevity regulates oxidative stress resistance and Mn-superoxide dismutase gene expression in Caenorhabditis elegans. FASEB J 13(11):1385–1393
68. Leite NR et al (2020) Baru pulp (Dipteryx alata Vogel): fruit from the Brazilian Savanna protects against oxidative stress and increases the life expectancy of Caenorhabditis elegans via SOD-3 and DAF-16. Biomolecules 10(8):1106
69. Uno M et al (2021) Neuronal DAF-16-to-intestinal DAF-16 communication underlies organismal lifespan extension in C. elegans. Iscience 24(7):102706
70. Libina N, Berman JR, Kenyon C (2003) Tissue-specific activities of C. elegans DAF-16 in the regulation of lifespan. Cell 115(4):489–502
71. Lazarou M et al (2015) The ubiquitin kinase PINK1 recruits autophagy receptors to induce mitophagy. Nature 524(7565):309–314
72. Shipley MM, Mangold CA, Szpara ML (2016) Differentiation of the SH-SY5Y human neuroblastoma cell line. J Vis Exp JoVE (108):e53193
73. Higham JP et al (2019) Alzheimer's disease associated genes ankyrin and tau cause shortened lifespan and memory loss in Drosophila. Front Cell Neurosci 13:260
74. Colbert HA, Bargmann CI (1995) Odorant-specific adaptation pathways generate olfactory plasticity in C. elegans. Neuron 14(4):803–812
75. Voglis G, Tavernarakis N (2008) A synaptic DEG/ENaC ion channel mediates learning in C elegans by facilitating dopamine signalling. EMBO J 27(24):3288–3299

Publisher's Note Springer Nature remains neutral with regard to jurisdictional claims in published maps and institutional affiliations.

Revised Proof